A98-31499

ICAS-98-2,3,2

Viscous Drag Optimization for a Transport Aircraft Mission Adaptive Wing

André Luiz Martins, M.Sc.
Fernando Martini Catalano, Ph.D.
Aircraft Laboratory
University of São Paulo, Brazil.

Abstract

A direct optimization study has been performed to produce a preliminary evaluation of the potential benefits of a mission adaptive wing employing variable camber technology in typical jet transport aircraft missions, in terms of fuel efficiency increase directly obtainable from airfoil viscous (pressure + friction) drag reduction alone. A 2-D airfoil analysis approach has been adopted, associated with an proposed idealized variable camber mechanism based on elastic deformation and surface extension. Using a direct function optimization program coupled to a viscous-inviscid airfoil analysis routine, optimized variable camber configurations were obtained for several of the decreasing weight conditions a typical transport aircraft faces along a cruise mission leg, due to fuel consumption. Independent runs have been executed considering only trailing and both leading and trailing edge camber variation and, for each of them, an integrated range parameter has been obtained, proportional to the maximum possible aircraft range. Results indicate that range increases up to 7.03% over the base airfoil could be reached with camber variation in the trailing edge region only, a figure that rose up to 24.6% when leading edge adaptation was considered simultaneously. However, pressure distribution results indicate that the high leading edge curvatures required for that would probably not be allowed by efficient supercritical cruise requirements. Coincidentally, on the other hand, the trailing edge only approach seems to offer a better substract for supercritical cruise.

List of Symbols

α	angle of attack (degrees)
ρ	atmospheric air density (kg/m^3).
δX, δZ	displacements in X and Z directions
a	speed of sound (km/h)
C	specific fuel consumption (1/h)
C_D	drag coefficient, $=D/(\frac{1}{2}\rho V^2 S)$
C_L	lift coefficient, $=L/(\frac{1}{2}\rho V^2 S)$
D	drag (N)
F	objective function
L	lift (N)
M	Mach number
P	airfoil perimeter (m)
R	aircraft range (km)
r	integrated range parameter
Re	Reynolds number
S	reference area (m^2).
W	aircraft weight (N)
w	weight parameter, $= M^2 C_L$
X_i	set of decision variables
X_{tr}	X transition position (m)

Subscripts

0, base	of the base airfoil
f	friction
max	maximum
opt	optimum
p	pressure
ref	reference

Abbreviations

ISA	International Standard Atmosphere
LE	airfoil leading edge
MAW	Mission Adaptive Wing
RP	reference point
TE	airfoil trailing edge
VCW	Variable Camber Wing

Introduction

Many concepts have been previously proposed to make the idea of real-time aerodynamic shape adaptation of an aircraft a feasible proposal from both technical and economical standpoints. Almost certainly, the mostly studied idea is the use of a Mission Adaptive Wing (MAW), in which wing geometric shape variation is applied to optimize the aircraft's aerodynamic performance for each situation of its flight. Variable sweep wings and even high-lift devices may be seen as MAW concepts in operation today.

Another widely researched MAW concept is the Variable Camber Wing (VCW), in which airfoil sections can have their camber line geometry locally modified, independently and smoothly in both spanwise and chordwise directions. An early implementation has been seen in the NASA AFTI/F-111 experimental aircraft[1], where the concept have proved to be able to improve cruise and maneuver performance in typical tactical fighter missions.

As noted by Gilyard and España[2], it is expected that any MAW concept would bring greater benefits for combat than for civilian transport

21st ICAS Congress
13-18 September 1998
Melbourne, Australia

aircraft, once the latter are designed and optimized considering much less flight variation along their missions, that is, mostly for high speed economical cruise. In spite of that, the potential gains of VCW technology in civilian operations have been seriously considered by leading manufacturers, due to their potential significance within a highly competitive market, marked by recession and globalization.

Research work on VCW technology applied to transport aircraft has been extensively reviewed by Fielding and Vaziry-Zanjany[3], who analyzed many previously obtained results against a maintenance and operation feasibility background. Encouraging DOC reductions were obtained for several of the operation environments modeled.

Taking this scenario into account, the present work has been proposed as an extension of previous research[4]. Its main objective is a preliminary evaluation of the potential benefits of VCW technology to enhance the fuel efficiency of jet transport aircraft by wing airfoil viscous (pressure and friction) drag reduction, at high speed, subsonic cruise flight conditions. Once defined a VCW airfoil model and other assumptions, the evaluation was performed by optimizing variable camber parameters for several stages along a typical transport aircraft mission. The optimization objective function is set to maximize an integrated airfoil range parameter, considered to be representative of the maximum possible variation of aircraft range due to viscous drag reduction.

Definition of the Optimization Problem

The optimization problem should translate, as well as possible, the efficiency adaptation of the variable camber airfoil into the real fuel efficiency increase a transport aircraft could obtain from the resulting viscous drag reduction, along a typical mission.

VCW technology is considered to be useful mostly in the cruise phase, during which a jet transport aircraft spends most of its fuel. In cruise, the aircraft's main source of inefficiency is its own weight reduction due to fuel consumption. Once a fixed geometry wing can be optimally designed for one set of weight and flight conditions only, transport aircraft usually cruise at off-design conditions.

To evaluate the cruise weight variation effect on range, one must take the integral form of the range equation[7] for a jet aircraft, expressed by:

$$\frac{RC}{a} = r = \int_{WN}^{W1} M \frac{L}{D} \frac{dW}{W} \qquad (1)$$

where indexes 1 and N indicate conditions at the start and at the end of the cruise phase, respectively.

It is evident that the maximization of the M(L/D) term at every point of the cruise leg maximizes the integrated range parameter **r**. Based on that, the optimization problem studied here can be stated with the following enunciate:

Given a typical jet transport aircraft cruise mission, find the set of variable camber wing parameters that optimize (maximize) the M(L/D) term for every weight condition found within the W_1 to W_N variation range, so maximizing the integrated range parameter ***r****.*

Obviously, the M(L/D) optimization described above should consider the whole aircraft drag variation due to VCW application, which includes, for example, trim, induced and fuselage upsweep drag effects. Nevertheless, the present work considers the optimization of the wing alone, from the standpoint that such results would represent the maximum potential benefits the wing itself would be able to offer in terms of viscous drag reduction, without considering eventual trade-offs with other sources of drag.

Based on the problem stated above, the following tasks have been established:

(a) To choose a variable camber wing representation model, with simplification and idealization levels compatible with a preliminary evaluation.

(b) To define the optimization/analysis methods to be used.

(c) To define typical jet transport mission conditions, represented by weight variation range and flow parameters.

The decisions and assumptions involved in the tasks set above are described in the following paragraphs.

Variable Camber Wing Representation Model

It has been decided that a simultaneously simplified and idealized modeling approach would be the most fruitful, for several reasons. A simplified model allows a fast evaluation of numerous conditions and a global vision of the problem, without eventual diversions that could be introduced with a modeling too sophisticated. On the other hand, the model should be representative of the optimization problem, also setting a solid base for future, more advanced analysis. With that in mind, an approach restricted to the two-dimensional airfoil domain has been chosen, representing a basic jet transport aircraft wing by a typical supercritical airfoil[6], displayed in Fig. 1.

Simplifications are also assumed in the representation of the flow. It is well known that most jet transport aircraft fly at high altitudes and at critical Mach numbers, taking advantage of the drag rise delaying characteristics of supercritical airfoils. Nevertheless, a complete characterization of such transonic flows would require complex analysis including, at least, non-linear compressibility and shock/boundary-layer interaction, considered to be beyond the scope of this work. So, it is assumed that high Mach number *subcritical* cruise conditions are still representative for viscous drag comparison purposes. This assumption is supported by the fact that the weak shock characteristics of supercritical airfoils do not significantly increase viscous drag even at critical conditions, when still below the drag rise Mach number.

An *idealized* model for the camber variation mechanism is also interesting due to the following factors: (a) the proposal of a really feasible VCW mechanism is considered far beyond the scope of this work, and also unnecessary for a preliminary evaluation; (b) A highly idealized mechanism would represent the outer envelope of possible solutions, that is, many possible "real world" VCW devices could be seen as some particular case, covered by the idealized model; (c) inexpressive benefits obtained with an idealized model would be a strong indication that a real mechanism would be even less effective, and possibly of no interest.

Based on that, the idealized variable camber mechanism proposed is presented in Fig. 2. As in previous VCW proposals[1-4], the mechanism assumes a central load carrying fixed section of the wing and two geometrically variable sections attached to it. Here the variable sections extend from the LE to 27.6% of the chord and from 64.5% of the chord to the TE (Fig. 2a).

The main idealization assumption for the mechanism is that shape variation could be entirely achieved by elastic deformation and length extension of the upper and lower surfaces of the variable sections. For this, two regions on the variable sections are considered to be "plugs", fixed in geometric shape to a certain extent of the chord from the LE and TE (Fig. 2a). It has been verified that the original airfoil could be closely reproduced by a single parametric cubic spline function, interpolating only the points on the fixed central section and on the LE and TE plugs. Arbitrary shape variation is then obtained through the following procedure:

(a) arbitrary displacement (δX, δZ) of LE and TE plugs, measured from an assumed reference point on each of them ("RP", Fig.2b);

(b) rotation of the plugs around the reference points. To keep minimum structural feasibility of the shape obtained, the rotation is assumed to be the slope of natural cubic spline curves, attached to the mean camber line of the central fixed section, and passing through each plug reference point (Fig. 2b);

(c) resampled airfoil representation by a single parametric cubic spline function, interpolating only the points on the LE and TE plugs and on the central fixed section. Fig. 2c shows an example resulting airfoil, discretized in 65 points and ready for aerodynamic analysis (Fig. 2c).

The cubic spline representation is considered to closely reproduce the possible shape the flexible variable sections would assume, given a certain plug displacement and rotation configuration. Also, it is observed that the airfoil exposed surface may actually be varied for an arbitrary displacement. A real mechanism that would possibly behave this way would be one in which the plugs push an pull flexible skins into and out of the central fixed section, through slots, while flexing the surfaces at the same time.

Analysis and Optimization Methods

Given the aerodynamic modeling assumptions, the airfoil analysis method by Williams[9] was adopted. The method uses an integral boundary layer method, extended to also calculate separated flow by assuming a two parameter description of the separated velocity profiles. The program is of the semi-inverse type, in which a direct inviscid calculation is coupled to an inverse calculation of the boundary layer. The outer inviscid flow is assumed to be both incompressible and irrotational, so that it can be described by the relevant solution of Laplace's equation, which is obtained by a surface singularity method. In the inner viscous flow, the laminar portion of the boundary layer is calculated by Thwaites' method and natural transition is predicted using Granville's correlation. If laminar separation occurs before transition, then the laminar separation bubble is calculated using Horton's semi-empirical technique. The development of the turbulent boundary layer and wake is calculated by the inverse formulation of Green's lag-entrainment method.

To control the overall optimization procedure, the optimizer program CONMIN, by Vanderplaats[10], was adopted. The program is coupled to the airfoil analysis routine, running it as a multivariable function evaluator. A chosen objective aerodynamic characteristic F (for example, M L/D) is declared dependent of a chosen set of decision variables $\{X_i\}$ (for example, VCW defining parameters). Using an iterative gradient method, the optimizer is able to numerically search for the set of decision variables values $\{X_i\}_{opt}$ which returns the minimum (or maximum) value of the objective

aerodynamic characteristic chosen $F(\{X_i\}_{opt})$. The final set of decision variables must be constrained to a certain domain by inequality equations, to ensure that the final result is feasible for the conditions required.

Typical Mission Conditions

To define typical cruise mission conditions, general data were obtained from Ref. 8 for several aircraft, considered to be representative for medium/short range jet transports. The following points deserve detailing:

(a) Atmospheric conditions at cruise were assumed to be those for ISA at 25.000 feet. However, high typical cruise Mach numbers could not be reproduced, due to the flow analysis limitations to subcritical flow, discussed above. Based on preliminary evaluations of the base airfoil (Fig. 1), a reference cruise Mach number of $M_{ref} = 0.575$ has been assumed, which assures subcritical conditions up to $C_L = 0.65$. The Reynolds number is calculated based on a MAC of 5 m, leading to a value of $Re = 32 \times 10^6$, for the base airfoil, a representative average for jet transport aircraft.

(b) Supposing a mission where all (non reserve) fuel is used, cruise weight fractions for that kind of aircraft have a lower limit of about:

$$W_N/W_1 = 0.75. \qquad (2)$$

This value was adopted here, once aircraft with larger weight variation will probably earn more benefits from VCW adaptation ability.

(c) A non-dimensional *weight parameter w* has been adopted to express weight whenever needed. Assuming a constant altitude cruise, weight can be written as:

$$W = \tfrac{1}{2}\rho a^2 S w\,, \text{ where } w = M^2 C_L \qquad (3)$$

Once most of the lift is generated by the wing, the aircraft C_L represents the average section c_L observed at any point across the span. So, for the present 2-D approach, the most representative choice is to consider the same *weight parameter* range ($w_2 \le w \le w_1$) for the airfoil alone. Although the complete design of a three-dimensional wing would obviously take spanwise variations into account, this assumption is considered representative enough to allow comparisons between conventional and VCW technologies, which are the focus of this work.

Numerical Optimization Scheme

Once the basic modeling, methods and overall optimization conditions were chosen, a numerical optimization scheme was implemented. A flow diagram showing the main procedures involved is presented in Fig. 3.

Initially, a discretized representation of weight parameter variation along the cruise mission must be established. The total weight variation interval $[w_1,w_N]$ is divided into (N-1) equal intervals, defining N different weight conditions w_i.

For each w_i weight parameter value, an optimization run is performed, where program CONMIN maximizes the airfoil M(L/D) parameter, using the airfoil analysis routine to evaluate the effect the available decision variables. The last may include any of the LE and TE variable camber geometry parameters and/or M itself. Given a certain parameter set, the VCW airfoil shape is calculated. The constraint of lift equal to weight ($w_i = M^2C_L$) is satisfied by adjusting the airfoil angle of attack, using a simple secant root finding method.

After the process is repeated for each w_i, $i = \{1,2,..,N\}$, the integral of Eq. 1 must be numerically evaluated, to obtain the integrated range parameter **r**. For that, the optimum $M(L/D)/w_i$ values are interpolated by a cubic spline function over the whole interval $[w_1,w_N]$ and integrated analytically. The resulting **r** value is then available for comparisons to the fixed airfoil range parameter, as well as to other optimization cases.

Definition of Optimization Cases

To have a better vision of "where" the viscous drag benefits obtainable with VCW technology may come from, two optimization cases were devised.

However, before any comparisons between conventional and VCW technologies can be made, it must be assured that an hypothetical fixed wing aircraft using the base airfoil chosen (Fig. 1), while flying at $M_{ref} = 0.575$, must have that airfoil operating at its best M(L/D) parameter for some weight w_c within its variation interval $[w_1,w_N]$.

To obtain w_c, a first optimization test run was executed. Considering an arbitrary weight parameter range discretized in N = 4 points, the fixed geometry of the base airfoil was kept, with only M as a decision variable. The results, presented in Fig. 4, were then interpolated for M = 0.575, resulting in $w_c = 0.1230$.

This value was then assumed to occur exactly at mid cruise weight, so it is the average of the extreme values w_1 and w_N. Considering the cruise weight fraction adopted (Eq. 2), a system of equations defines the extreme weight values, as follows:

$$\left.\begin{array}{l} \dfrac{w_1 + w_N}{2} = w_c = 0.1230 \\ \dfrac{w_N}{w_1} = 0.75 \end{array}\right\} \begin{array}{l} w_1 = 0.1406 \\ w_N = 0.1055 \end{array} \quad (4)$$

It can be observed that, if a constant Mach number of M = Mref = 0.575 is kept, the relation from Eq. 3 yields an expected C_L range $[C_{L1}, C_{LN}]$, where:

$$C_{L1} = w_1 / M_{ref}^2 = 0.4253$$
$$C_{LN} = w_N / M_{ref}^2 = 0.3189 \quad (5)$$

That cruise C_L range is closely compatible with those observed for typical jet transport aircraft[8].

Once defined the weight parameter interval $[w_1, w_N]$ which is mid divided by the best operation point w_c of the base airfoil, the optimization cases were set, representing two possible combinations of decision variables involving variable LE and TE camber parameters, as displayed in Tab. 1.

		Decision Variables	
	Case	δxTE, δzTE	δxLE, δzLE
1	TE	yes	no
2	LE+TE	yes	yes

Table 1 – Optimization Cases

It is seen that, although the method is able to handle M as a variable, no such condition has been studied (other than the first test run, necessary to define w_c). This has been decided because typical jet transport aircraft engines usually have specific fuel consumption factors C very sensitive to flight speed, and so are expected to work within a tight M variation range, around an optimum consumption point. Once C has been previously assumed as a constant (Eq. 1), the inclusion of M variation has been considered useless and left for future research, when a model for C variation would eventually allow any C x M trade-off studies. Given that, the reference value M = 0.575 is always assumed.

For all cases studied, the weight range was discretized into four equal segments, defining the five point interval $[w_1, w_5]$ (N=5).

Finally, two constraints are imposed: (a) the maximum local Mach number at any point over the airfoil surface M_{max} must never exceed 0.95 and (b) the total perimeter P of the airfoil must never be less than 0.99 times that of the original base airfoil, P_0. These restrictions are put in terms of two functions submitted to inequations:

$$G(1) = M_{max} - 0.95 \le 0$$
$$G(2) = 1.0 - \frac{P}{P_0} \le 0 \quad (6)$$

Results and Discussion

Figures 5 to 17 present several results obtained for the two optimization cases run, which are compared to the base airfoil data, obtained under the same weight range and flow conditions described above. The data are discussed below, for each case separately.

Case 1: Trailing Edge Variable Camber

The resulting TE variable camber shapes obtained for three of the five weight values w_i within the range defined (Eq. 4) are displayed in Fig. 5. The gradual reduction of camber curvature from the highest weight w_1 to the lowest w_5 can be clearly observed, as well as the α variation needed to cope with the weight constraint ($w_i = M^2 C_L$).

Fig. 6 gives an indication of the L/D increase obtained with the geometry adaptation, in relation to the fixed airfoil. However, it is believed that the variation of the integrand term of the range equation M(L/D)/w (Eq. 1) in Fig. 7 gives a clearer indication of what that efficiency increase means in terms of potential increase in integrated range parameter **r** (area below each curve). As indicated, an increase of Δr = +7.03% is expectable.

Figure 8 presents the estimated boundary layer transition position X_{tr}/c, for both upper and lower surfaces of the adaptive TE and fixed base airfoils. It is clear that the total (upper plus lower) extension of laminar flow is reduced for every weight parameter. In contrast to the increase in L/D observed (Fig. 5), this result indicates that possibly a friction x pressure drag trade-off has occurred.

That trend is confirmed by the data from Fig. 15, which displays the estimated values of pressure (C_{Dp}) and friction (C_{Df}) drag coefficients separately, as well as their sum ($C_D = C_{Dp} + C_{Df}$), all against the C_L values limiting the weight range (Eq. 5). The optimization clearly indicates that, for the weight parameter range, base airfoil geometry and flow conditions studied, it may be interesting to pay a small price in friction drag, which may lead to a larger relative reduction in pressure drag, thus minimizing total C_D.

Case 2: Simultaneous Trailing and Leading Edge Variable Camber

Fig. 9 and 10 present the resulting optimized geometries for the LE and TE simultaneously variable camber case, for three weight parameter values within the range $[w_1, w_5]$. The main feature evident in Fig. 9 is the intense downward curvature at the leading edge, probably adapting the stagnation point around it to an ideal position. Also, a gradual reduction of LE curvature with reduction of weight is clearly seen. Less obvious is the upward curvature of the trailing edge,

displayed in Fig. 10, also gradually intensified by increasing weight.

Fig. 11 presents the resulting L/D increase observed within $[w_1,w_5]$, clearly superior to both the base airfoil and the previous case. The correspondent curves of the M(L/D)/w range parameter integrand are displayed in Fig. 12, indicating a variation Δr = 24.6% over the base airfoil, adding a 16.4% increase over Case 1.

Fig. 13 indicates that the optimized configurations resulted in a total laminar boundary layer extents (X_{tr}/c) even shorter than that observed for Case 1 (Fig. 8), in spite of the large increases observed in L/D. Part of this effect is explained by a partial reduction of wetted area, within the 1% margin allowed by constraint G(2) (Eq. 6) and evident in Fig. 9. However, that result still favors the pressure x friction drag trade-off hypothesis, this time confirmed by Fig. 16. The C_{Dp} reduction reached is larger than that for Case 1, and C_{Df} is also smaller, reaching values similar to those of the base airfoil. A comparison of those magnitudes is presented in Fig. 14, in terms of percentile drag variations relative to the base airfoil values ($\Delta CD = (C_D-C_{Dbase})/C_{Dbase}$).

Pressure Distributions

Results in terms of pressure distributions are displayed in Fig. 17, for the base airfoil and Case 1 and Case 2 optimized geometries, all for the highest loading condition of $w = w_1$, $C_L = C_{L1}$ = 0.425. Along with the data there are profile representations (approximately to scale) of the referent airfoils, all of them rotated by α relative to the horizontal lines drawn (meaning that the freestream velocity is parallel to the horizontal lines).

One first interesting feature observed is the shape of the pressure distribution for the Case 2 airfoil, where LE adaptation smoothes down the upper surface suction peak seen on the base airfoil, bringing it to a more downstream position along the chord, thus largely alleviating the C_P gradient after it. Apparently, the price paid for that is the appearance of a lower surface pressure peak at roughly the same chordwise position, and a consequent pressure gradient inversion that do not occur for the base airfoil, explaining the premature local BL transition (Fig. 13).

For the Case 1 airfoil, it is observed that a large suction peak reduction also occurs, although the unaltered LE curvature leaves it at roughly the same chordwise position. It can be seen that the Case 1 airfoil becomes "after-loaded", with the expected pressure difference increase around the curved TE.

Finally, an interesting and surprising "lateral effect" observation can be made: although taking only viscous drag considerations into account, the optimized result of Case 1 (TE only) tends to offer better transonic qualities than the base airfoil for the same condition. That is indicated in the flatter upper surface C_P distribution that is generated in Case 1, which could possibly favor the formation of weaker shocks at higher Mach numbers. Comparing the base airfoil and the Case 1 optimized shape in Fig. 16, it can be seen that the latter has the LE of the airfoil at a much favorable angle of attack, offering its upper surface less deviated from the freestream. It is also evident that such behavior is coincidental, once the Case 2 (LE+TE) results depart from that trend, in spite of its greater number optimization degrees of freedom. Such departure is also evident in Case 2 resulting shape and angle of attack (Fig. 16) which evidently demonstrates a trend to become a typically subcritical airfoil.

In summary, the observations made indicate that, under real supercritical cruise constraints, LE variable camber deflections are expected to be much less intense than the ones observed for Case 2.

Conclusions

Under the modeling simplifications and idealizations assumed, it is believed that the main objectives of this work were accomplished, allowing a first evaluation of the potential wing airfoil viscous drag reduction benefits reachable with the use of VCW technology, under typical jet transport operation conditions. Based on the results obtained and presented above, the following conclusions may be drawn:

(a) Within the limitations of the airfoil analysis method, it has been concluded that the idealized variable camber mechanism proposed would be able to considerably reduce wing airfoil viscous drag along the cruise leg of a typical jet transport aircraft. Translated into an integrated range parameter (Eq. 1) along the same weight variation interval, those reductions indicated a potential increase in range of 7.03% with the application of variable camber at the TE region only, a variation that increased to 24.6% when geometry adaptation was applied also to the LE region.

(b) The optimized geometry results (Fig. 5, 9 and 10) and the estimated potential range increases indicate that camber adaptation at the LE region is more significative for *viscous drag* reduction than at the TE. On the other hand, the results of the optimization of the TE region only (Case 1) coincidentally lead to pressure distributions much more favorable for transonic conditions, that is, with gradients close to zero along the upper surface (Fig. 16). Such coincidental

confrontation of viscous drag and supercritical conditions indicates that probably much less LE curvature would be desirable at supercritical conditions, and introduces the question of whether it would be needed at all. This questioning is important when viewed from the standpoint of possibly easier mechanical implementation of the variable camber solution at the TE only, suggesting a future trade-off study.

(c) It has been observed that, at least for the particular base airfoil adopted (Fig.1) and for the conditions assumed, viscous drag reductions within the cruise leg would occur entirely in terms of pressure drag. The friction drag component for optimized VCW geometries was kept roughly the same (Case 2, LE+TE) or even larger than (Case 1, LE) that of the base airfoil, in favor of a pressure drag reduction of much larger magnitude. It is recognized that the explanation of such results may lie somewhere between reality, the limitations of the analysis method and the choosing of the base airfoil (Fig.1) as a representative typical one. Whatever is the case, the results suggest the need for deeper future studies involving other base airfoils and analysis methods.

Finally, an important point that must be reminded about the results obtained is the fact that, besides being limited by all the assumptions made, they only take *airfoil viscous drag* considerations into account, analyzing its reduction without considering any trade-offs with other sources of aerodynamic drag. However, the present results give some indication of *how much* viscous drag reduction could be achieved under idealized conditions and typical operation conditions, thus setting an upper limit to the expectations in that respect. Also, this study demonstrates some evidence that supercritical flight conditions would not allow the large LE deflections indicated for viscous drag minimization, opening the question for a future trade-off study, confronting viscous drag and supercritical conditions in a balance that seems to be more sensitive than expected before.

Future Work

The inherent limitations and some problems observed with the present work have suggested several points for progress in future research.

By the time of this writing, work is underway to reproduce the results presented here by using a genetic optimization algorithm[11]. The main reason for this is that, although initially thought to offer lower computational costs, the gradient search optimization method employed, required tight tolerance parameters to cope with the highly sensitive airfoil problem, a measure which apparently increased computation expense. Because of that, a "cost x robustness" comparison between the genetic and the gradient approach is considered important for future work, paving the way for considering more complex geometry and phenomena, involving a higher number of decision variables.

As mentioned in the above conclusions, a following natural suggestion will be to compare different airfoil analysis methods, applied to different base airfoils. Finally, an interesting next step would be to attack the problem of the trade-off between viscous drag reduction and favorable supercritical characteristics of the airfoil, an important question risen by the present work and which may even define the need for and/or the viability of complex leading edge camber variation mechanisms in transport aircraft.

References

1. Powers, S.G.; Webb, L.D.: *Flight Wing Surface Pressure Measurements and Boundary-Layer Data from the F-111 Smooth Variable-Camber Supercritical Mission Adaptive Wing.* NASA TM 4789, 1997.
2. Gilyard, G.; España, M.: *On the Use of Controls for Subsonic Transport Performance Improvement: Overview and Future Directions.* NASA TM 4605, 1994.
3. Fielding, J. P.; Varziry-Zanjany, M.A.F.: *Reliability, Maintainability and Development Cost Implications of Variable Camber Wings.* Aeronautical Journal, May, 1996. p. 183-195
4. Martins, A.L.; Catalano, F.M.: *Aerodynamic Optimization Study of a Mission Adaptive Wing for Transport Aircraft.*
5. Martins, A.L.; Ribeiro, R.S.: *Aircraft Induced Drag Minimization Using a Constrained Optimization Method.* 20th Congress of the International Council of Aeronautical Sciences (ICAS 96), Italy, 1996.
6. McKinnon, A.V.: *An Experimental Study of a Variable Camber Wing.* Ph.D. Thesis, Cranfield Institute of Technology, UK, October, 1993.
7. Raymer, D.P.: *Aircraft Design: a Conceptual Approach.* AIAA Education Series, 1989.
8. Torenbeek, E.: *Synthesis of Subsonic Airplane Design.* Delft University Press, 1982.
9. Williams, B.R.: *The Prediction of Separated Flow Using a Viscous-Inviscid Iteration Method.* R.A.E. Tech. Memo. Aero 2010, 1984.
10. Vanderplaats, G. N.: *CONMIN - A FORTRAN Program for Contrained Function Minimization.* NASA TM X-62282, Ames Research Center, 1973.
11. Goldberg, D. E.: *Genetic Algorithms in Search, Optimization and Machine Learning.* Addison-Wesley, 1989.

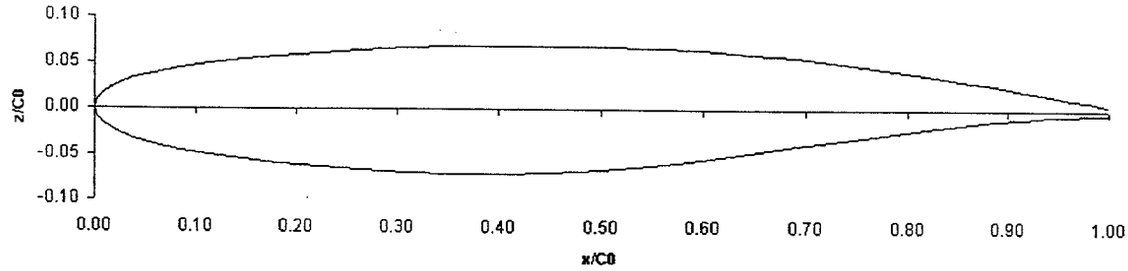

Figure 1 – Base Airfoil (Ref. 6)

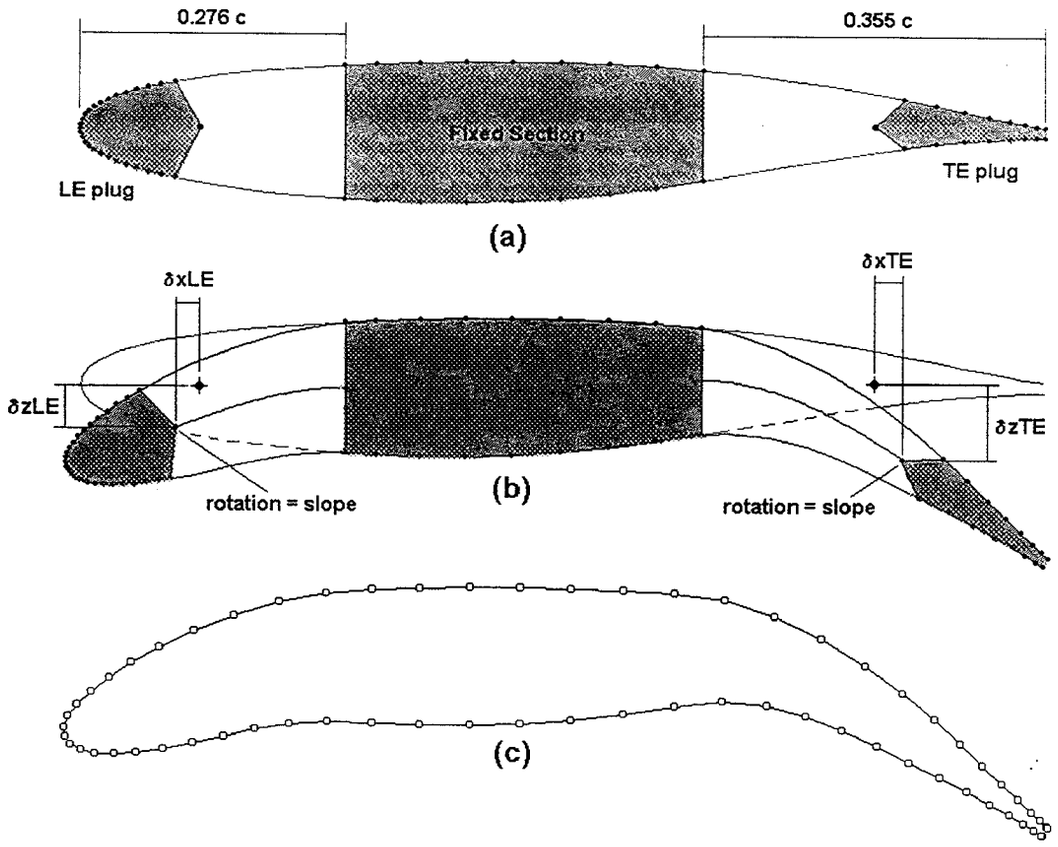

Figure 2 – Idealized camber variation scheme:
(a) Undeformed base airfoil.
(b) Plug displacement and rotation.
(c) Airfoil shape resampling (65 points).

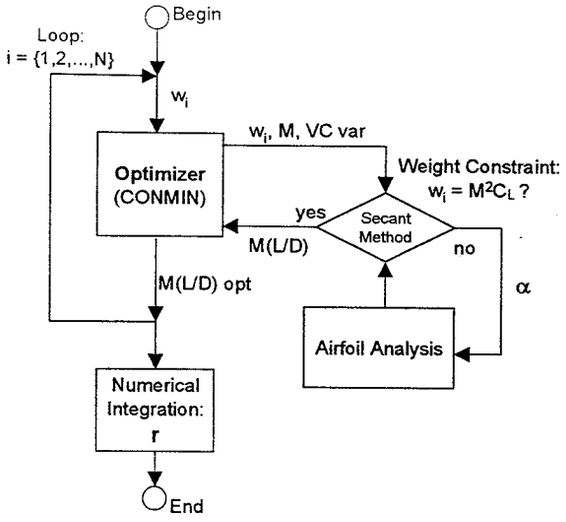

Figure 3 – Numerical optimization scheme: flow diagram.

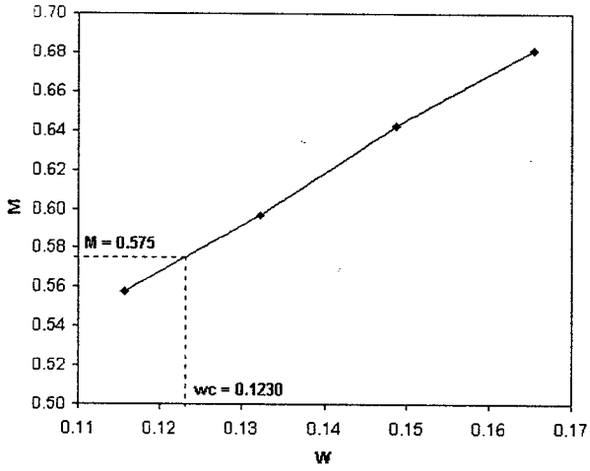

Figure 4 – First optimization test run and interpolation for w_c.

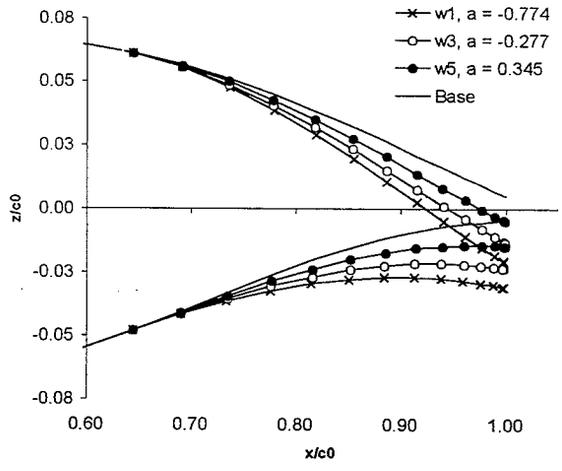

Figure 5 – Optmized TE airfoil shapes and α values, Case 1 (TE only).

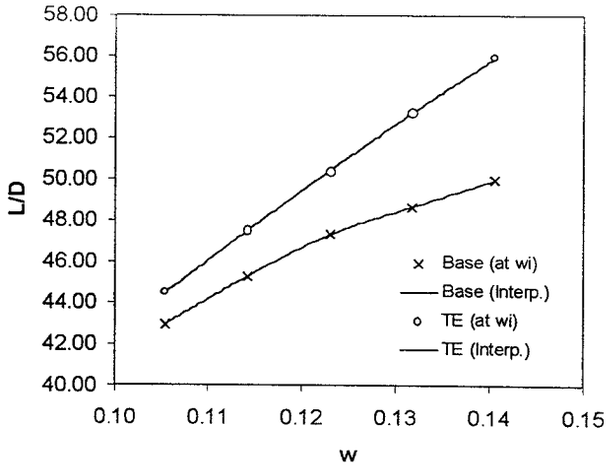

Figure 6 – L/D for base and optimized airfoils, Case 1 (TE only)

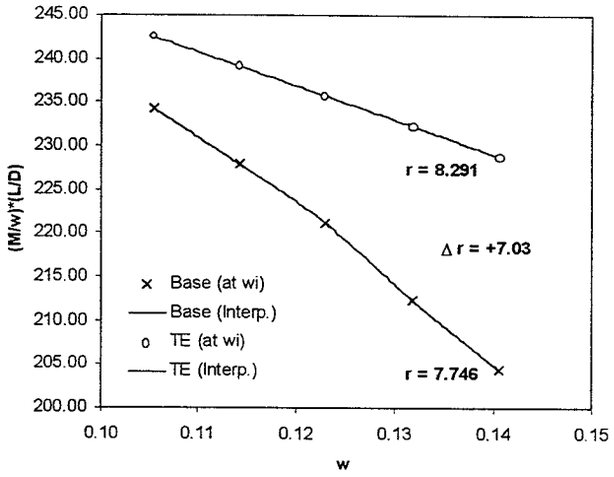

Figure 7 – M(L/D)/w for base and optimizedairfoils, Case 1 (TE only)

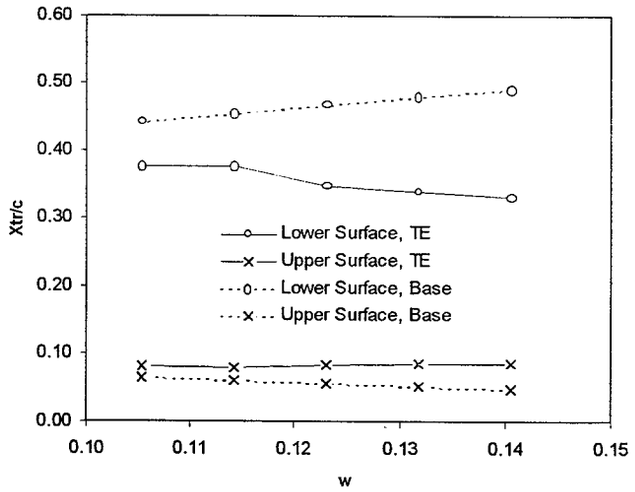

Figure 8 – B.L. transition position for base and optimized airfoils, Case 1 (TE only)

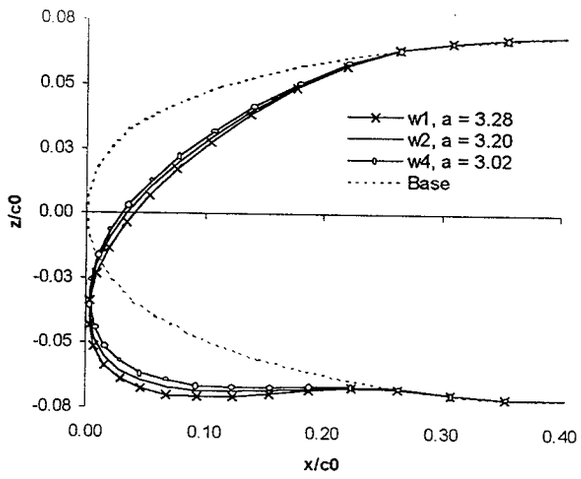

Figure 9 –Optmized LE airfoil shapes and α values, Case 2 (LE+TE).

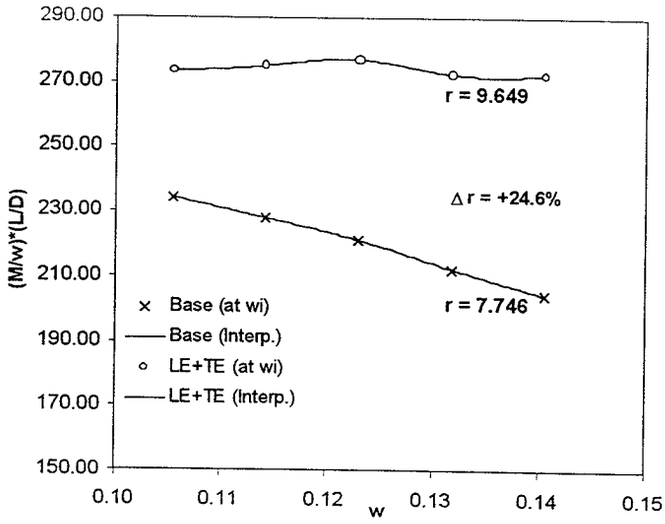

Figure 12 – M(L/D)/w for base and optimized airfoils, Case 2 (LE+TE)

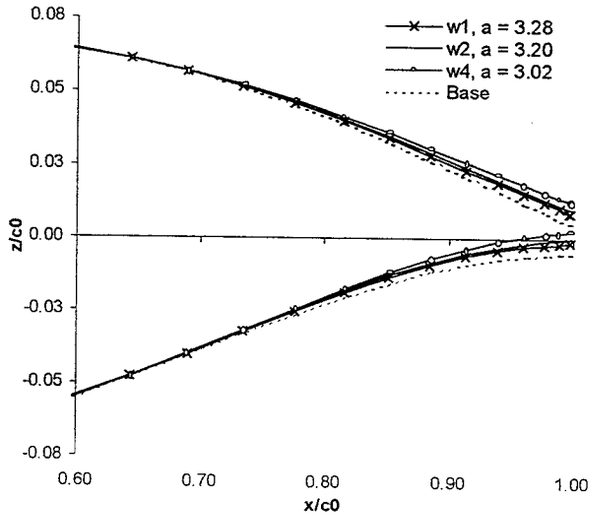

Figure 10 –Optmized TE airfoil shapes and α values, Case 2 (LE+TE).

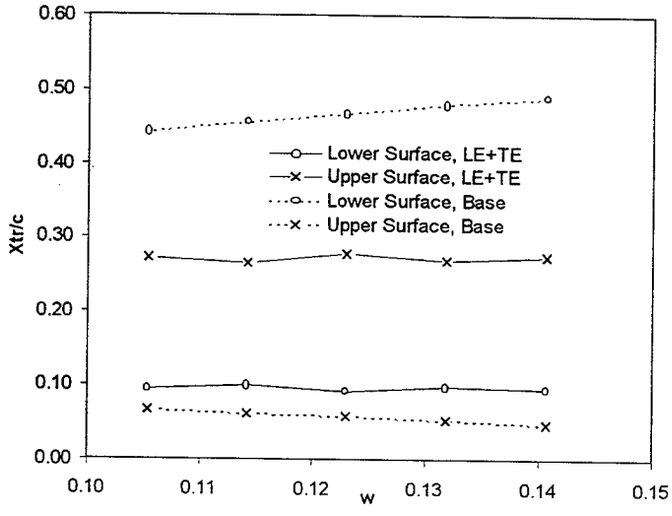

Figure 13 – B.L. transition position for base and optimized airfoils, Case 2 (LE+TE)

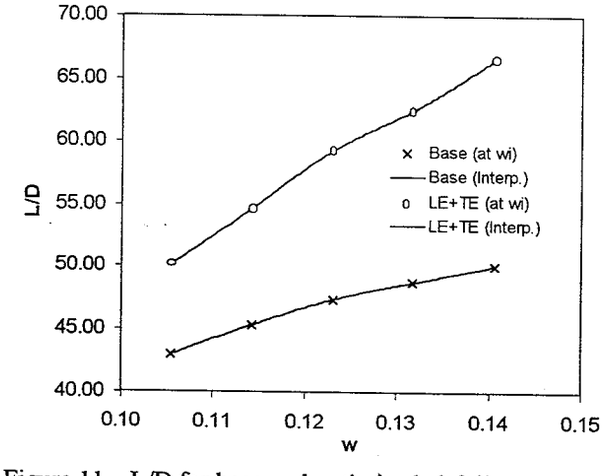

Figure 11 – L/D for base and optimized airfoils, Case 2 (LE+TE)

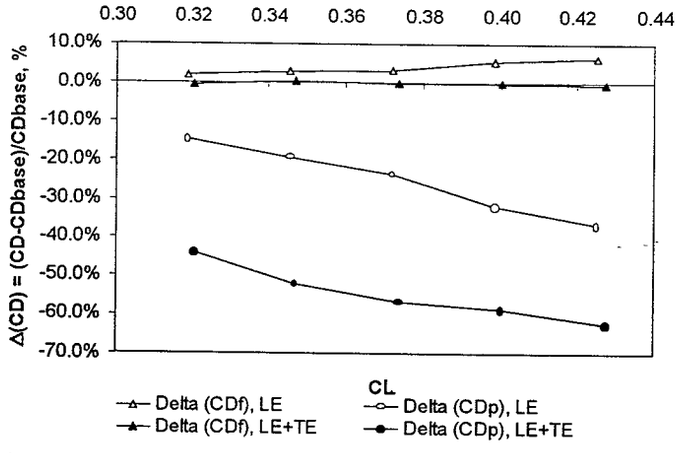

Figure 14 – Percentile variations in friction and pressure drag, relative to base airfoil, Cases 1 and 2.

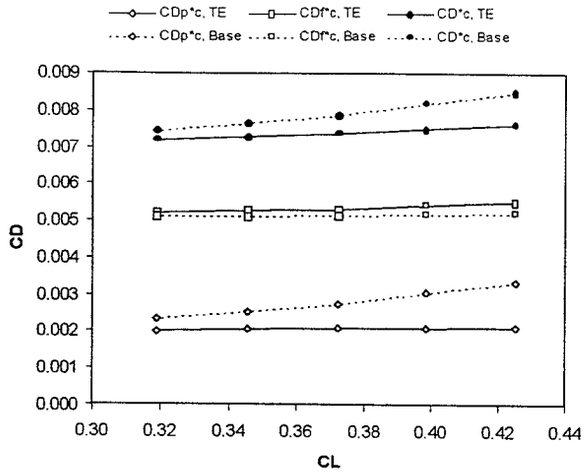

Figure 15 – Drag coefficient values within cruise C_L range, base and optimized airfoils, Case 1 (TE only)

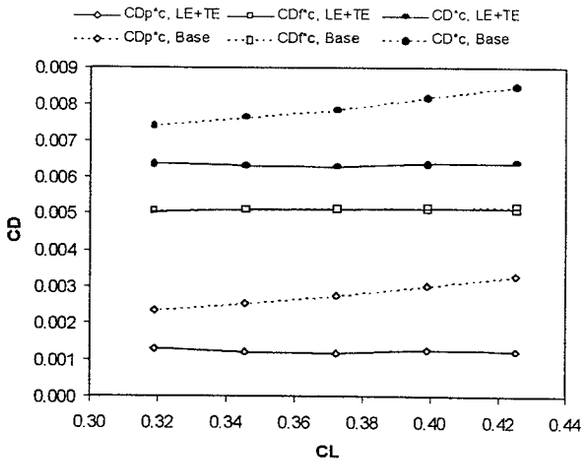

Figure 16 – Drag coefficient values within cruise C_L range, base and optimized airfoils, Case 2 (LE+TE)

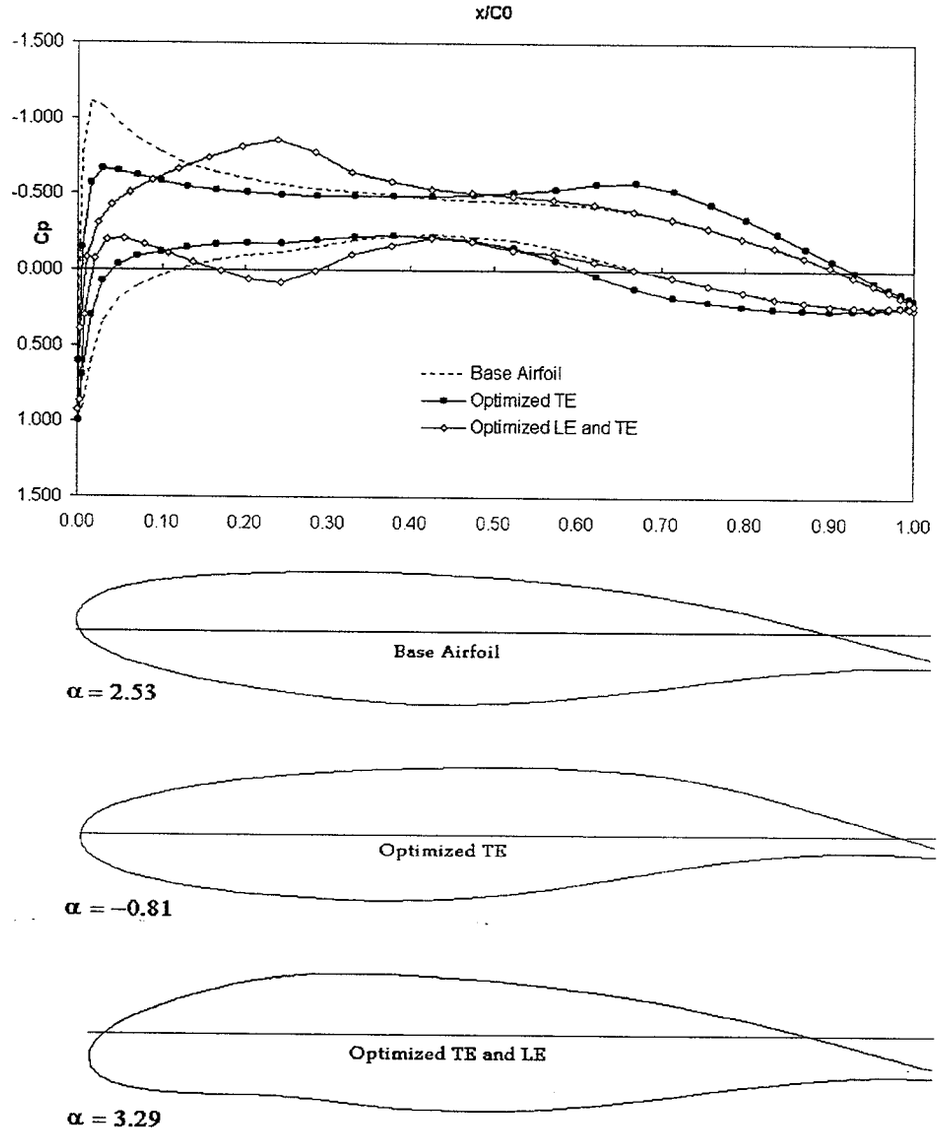

Figure 17 – C_P values (for w = w1, C_{L1} = 0.425) and profiles for base and optimized airfoils (rotated by α).